AGU PUBLICATIONS

Geophysical Research Letters

RESEARCH LETTER
10.1002/2015GL065004

Special Section:
First Results from the MAVEN Mission to Mars

Magnetic reconnection in the near-Mars magnetotail: MAVEN observations

Y. Harada[1], J. S. Halekas[2], J. P. McFadden[1], D. L. Mitchell[1], C. Mazelle[3,4], J. E. P. Connerney[5], J. Espley[5], D. E. Larson[1], D. A. Brain[6], L. Andersson[6], G. A. DiBraccio[5], G. A. Collinson[5], R. Livi[1], T. Hara[1], S. Ruhunusiri[2], and B. M. Jakosky[6]

[1]Space Sciences Laboratory, University of California, Berkeley, California, USA, [2]Department of Physics and Astronomy, University of Iowa, Iowa City, Iowa, USA, [3]CNRS, IRAP, Toulouse, France, [4]Paul Sabatier University, Toulouse, France, [5]NASA Goddard Space Flight Center, Greenbelt, Maryland, USA, [6]Laboratory for Atmospheric and Space Physics, University of Colorado Boulder, Boulder, Colorado, USA

Key Points:
- We present comprehensive MAVEN observations of magnetic reconnection at Mars
- The observed signatures are consistent with previous multispecies PIC simulations
- Mars provides a unique environment for investigation of multi-ion reconnection

Correspondence to:
Y. Harada,
haraday@ssl.berkeley.edu

Citation:
Harada, Y., et al. (2015), Magnetic reconnection in the near-Mars magnetotail: MAVEN observations, *Geophys. Res. Lett., 42*, doi:10.1002/2015GL065004.

Received 18 JUN 2015
Accepted 2 AUG 2015

Abstract We report Mars Atmosphere and Volatile EvolutioN (MAVEN) observations of electrons, ions, and magnetic fields which provide comprehensive demonstration of magnetic reconnection signatures in the Martian magnetotail. In the near-Mars tail current sheet at $X_{MSO} \sim -1.3R_M$, trapped electrons with two-sided loss cones were observed, indicating the closed magnetic field topology. In the closed field region, MAVEN observed Hall magnetic field signatures and Marsward bulk flows of H^+, O^+, and O_2^+ ions, which suggest the presence of X lines tailward from the spacecraft. Velocity distribution functions of the reconnection outflow ions exhibit counterstreaming beams separated along the current sheet normal, and their bulk velocities in the outflow direction inversely depend on ion mass. These characteristics are in qualitative agreement with previous multispecies kinetic simulations. The near-Mars magnetotail provides a unique environment for studying multi-ion reconnection.

1. Introduction

Magnetic reconnection is a fundamental process in space plasmas that changes magnetic field topology and converts magnetic energy into particle energy. Its possible occurrence, detailed physical processes, and global consequences in the Martian plasma environment are one of the key unaddressed issues relevant to Mars science, because reconnection may play a crucial role in controlling the particle acceleration and atmospheric loss processes from Mars [*Krymskii et al.*, 2002; *Brain*, 2006; *Brain et al.*, 2010; *Halekas et al.*, 2011]. One likely location for reconnection occurrence is provided by the central tail current sheet in the Martian-induced magnetotail formed as a result of the solar wind interaction with the Martian exosphere and ionosphere [*Nagy et al.*, 2004; *Halekas and Brain*, 2010].

The presence of magnetic reconnection at Mars has been discussed in terms of Hall magnetic fields [*Eastwood et al.*, 2008; *Halekas et al.*, 2009], electron signatures [*Brain et al.*, 2006, 2007], and magnetic flux ropes [*Brain et al.*, 2010; *Briggs et al.*, 2011; *Beharrell and Wild*, 2012; *Hara et al.*, 2014a, 2014b]. However, the lack of simultaneous measurements of ions and magnetic fields by modern instrumentation at Mars has hindered direct confirmation of Alfvénic accelerated plasma flows within current sheets, which are often thought of as the clearest evidence of magnetic reconnection [*Paschmann et al.*, 2013]. Given the common presence of tailward ion flows accelerated by nonreconnection processes in the Martian magnetotail [*Lundin*, 2011; *Dubinin et al.*, 2012a], Marsward ion flows confined within a current sheet would provide the most definitive evidence for reconnection bulk acceleration in the Martian tail current sheet, as observed in the Venusian magnetotail [*Zhang et al.*, 2012; *Dubinin et al.*, 2012b, 2013].

In this paper, we report magnetic reconnection signatures in the near-Mars magnetotail observed by the Mars Atmosphere and Volatile EvolutioN (MAVEN) mission [*Jakosky et al.*, 2015]. Simultaneous measurements of ions, electrons, and magnetic fields by the state-of-the-art instruments with proper time, energy, angle, and mass resolutions provide us with the most complete data sets ever which suggest the presence of magnetic reconnection at Mars. The observed reconnection signatures include the closed magnetic field topology in the central tail current sheet, Hall magnetic fields, Marsward ion bulk flows with counterstreaming beams in the

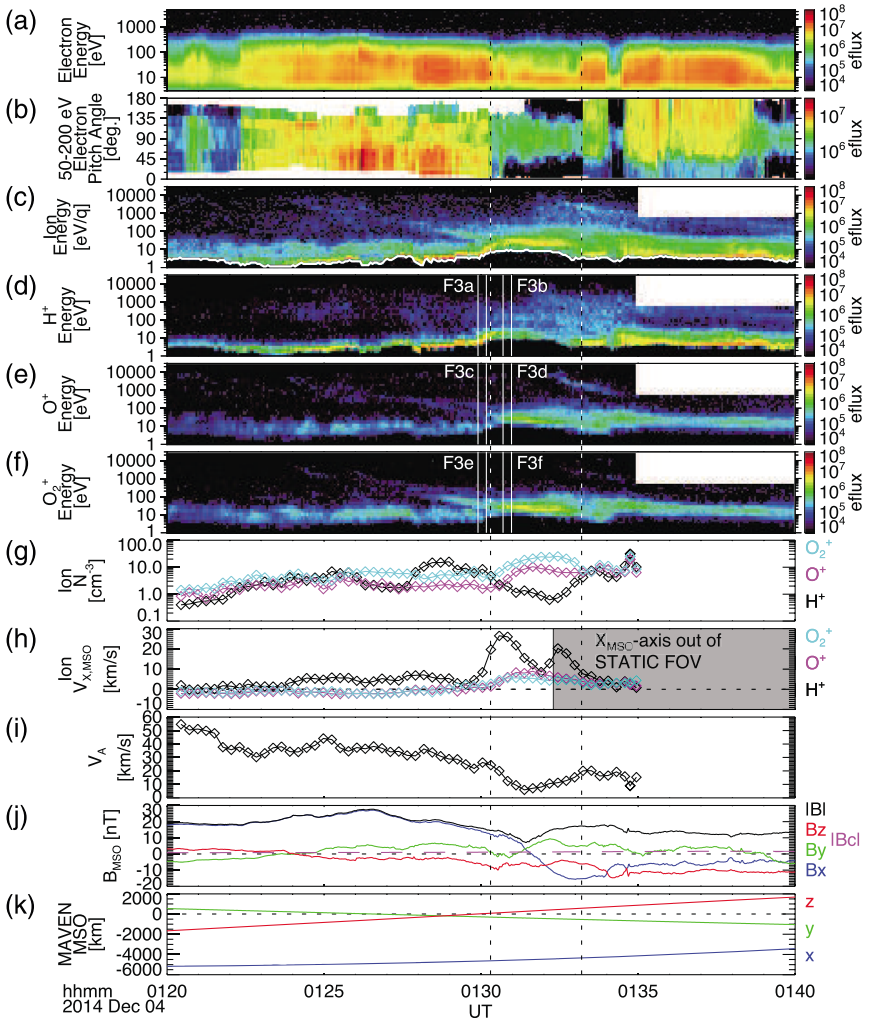

Figure 1. Time series data obtained by MAVEN on 4 December 2014. (a) Electron energy and (b) pitch angle spectra from SWEA, energy spectra of (c) all, (d) H^+, (e) O^+, and (f) O_2^+ ions, (g) ion densities, and (h) X_{MSO}-component of ion velocities from STATIC, (i) Alfvén velocity $V_A = B/\sqrt{\mu_0 \rho_i}$, where ρ_i is the total ion mass density, (j) magnetic field in the MSO frame from MAG, and (k) spacecraft MSO coordinates. Energy and pitch angle spectra are shown in units of differential energy flux (eflux) of eV/cm^2/str/s/eV. The white line in Figure 1c represents the minimum ion energy which is used to infer negative spacecraft potentials. The shadowed area in Figure 1h denotes the time interval when the X_{MSO} axis is out of the STATIC field of view and $V_{x,MSO}$ is less reliable. The magenta dashed line in Figure 1j shows the crustal field strength $|B_c|$ computed from the spherical harmonic model [*Morschhauser et al.*, 2014]. The vertical dashed lines denote the time interval when the electron spectra suggest closed magnetic field topology (suppressed flux of hot electrons with two-sided loss cone distributions). The vertical white lines in Figures 1d–1f and labels F3a–F3f show the time intervals from which the slices of ion velocity distributions are generated in Figures 3a–3f.

closed field region, and the coexistence of cold ion inflow and Marsward O_2^+ ion beam with energy dispersion in the separatrix region.

2. Observations

Figure 1 shows MAVEN observations of electrons from Solar Wind Electron Analyzer (SWEA) [*Mitchell et al.*, 2014], ions from Suprathermal And Thermal Ion Composition (STATIC) [*McFadden et al.*, 2014], and magnetic fields from Magnetometer (MAG) [*Connerney et al.*, 2014] in the near-Mars magnetotail ($-1.6R_M < X_{MSO} < -1R_M$, where R_M is the Mars radius) at 01:20:00–01:40:00 UT on 4 December 2014. During this time interval, STATIC observed three major ion species of the Martian magnetosphere: H^+ (Figure 1d), O^+ (Figure 1e), and O_2^+ (Figure 1f). The spacecraft was located in shadow throughout this time interval, and the negative spacecraft potential is estimated from the minimum ion energy, which is shown by the white line in Figure 1c.

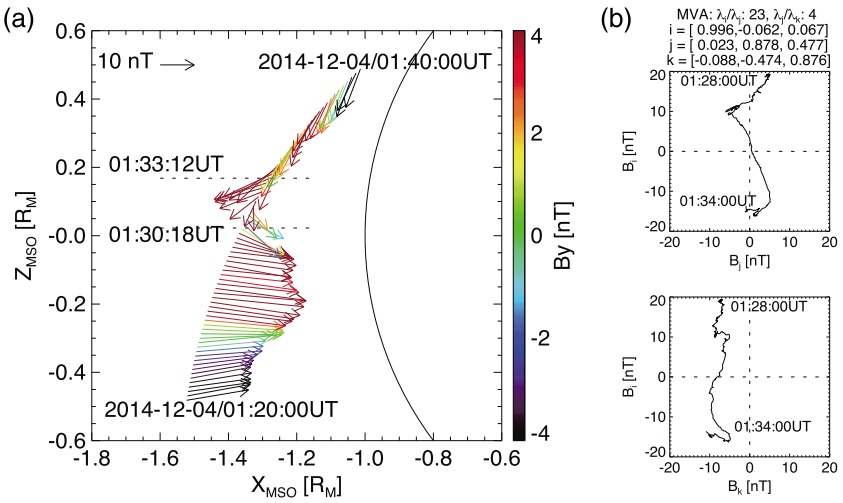

Figure 2. (a) Local magnetic field vector projected on the X_{MSO}-Z_{MSO} plane. The arrow colors show the out-of-plane B_y component. The horizontal dashed lines correspond to the vertical dashed lines in Figure 1. (b) Hodograms of magnetic field components in minimum variance coordinates.

The ion moments of the three species (Figures 1g and 1h) are computed from the three-dimensional distribution function of each species after correcting for the spacecraft potential (i.e., shifting energy in units of distribution function), and the spacecraft velocity is taken into account in the bulk ion velocity in the Mars Solar Orbital (MSO) frame. Figure 2a shows the magnetic field vector projection at the observed location on the X_{MSO}-Z_{MSO} plane with colors representing the out-of-plane B_y component. The subsolar longitude in the Mars body-fixed frame was ~50°E at this time. The upstream solar wind density, speed, and interplanetary magnetic field (IMF) were 3.9 cm^{-3}, 558 km/s, and [0.7, −0.4, 2.8] nT in MSO coordinates at 00:04:00 UT immediately before the inbound entry into the magnetosheath, and 4.3 cm^{-3}, 577 km/s, and [0.6, 2.0, −1.6] nT at 02:37:00 UT immediately after the outbound exit from the magnetosheath, based on Solar Wind Ion Analyzer (SWIA) [*Halekas et al.*, 2013] and MAG measurements. The IMF was significantly tilted from the ecliptic plane with the dominant northward component before the entry, and the B_z sign flipped sometime during the MAVEN tail crossing. Overall, the upstream solar wind driver provides a moderately high dynamic pressure of ~2 nPa with variable IMF at this time.

MAVEN crossed the central tail current sheet at 01:31:26 UT, which is identified as the B_x reversal in Figures 1j and 2a. The spacecraft longitude in the Mars body-fixed frame was ~124°W at this time. This current sheet crossing is accompanied by a bipolar B_y signature changing from negative (dawnward) to positive (duskward) values. The predicted crustal field strength is vanishingly small at this altitude as shown by the magenta dashed line in Figure 1j. Meanwhile, the electron distributions display significant changes in energy spectra (Figure 1a) and in pitch angle distributions (Figure 1b) around the current sheet crossing. The vertical dashed lines denote the timing at which we observe significant changes in the electron distributions. Before the first vertical dashed line at 01:30:18 UT, SWEA generally measured the large flux of parallel electrons with pitch angles <90° and loss cones in the antiparallel side as long as SWEA's field of view covered most of the pitch angles >90° (Figure 1b). The latter indicates that the magnetic field line is connected to the Martian atmosphere on the parallel side [*Brain et al.*, 2007], which is consistent with the magnetic field geometry (Figure 2a). Between the two vertical dashed lines at 01:30:18–01:33:12 UT, the hot electron flux is suppressed (Figure 1a) and the pitch angle distributions exhibit two-sided loss cones (Figure 1b). These signatures are associated with electron trapping in the closed field lines with both ends connected to the electron-absorbing atmosphere. After the second vertical dashed line at 01:33:12 UT, we observe loss cones at the parallel side as well as intermittent two-sided loss cones at 01:34:04–01:34:36 UT and after 01:38:42 UT (Figure 1b). This indicates that the field lines in this region are connected to the Martian atmosphere at the antiparallel end, which is again consistent with the geometry (Figure 2a), and that occasionally the parallel end is also connected to the atmosphere, suggesting complicated filed line topology. After this time interval, the B_x reversed its sign again from negative to positive at 01:41:26 UT (not shown), suggesting dynamically evolving and/or spatially complex magnetotail structures deviated from the static two-lobe configuration. The observed closed field

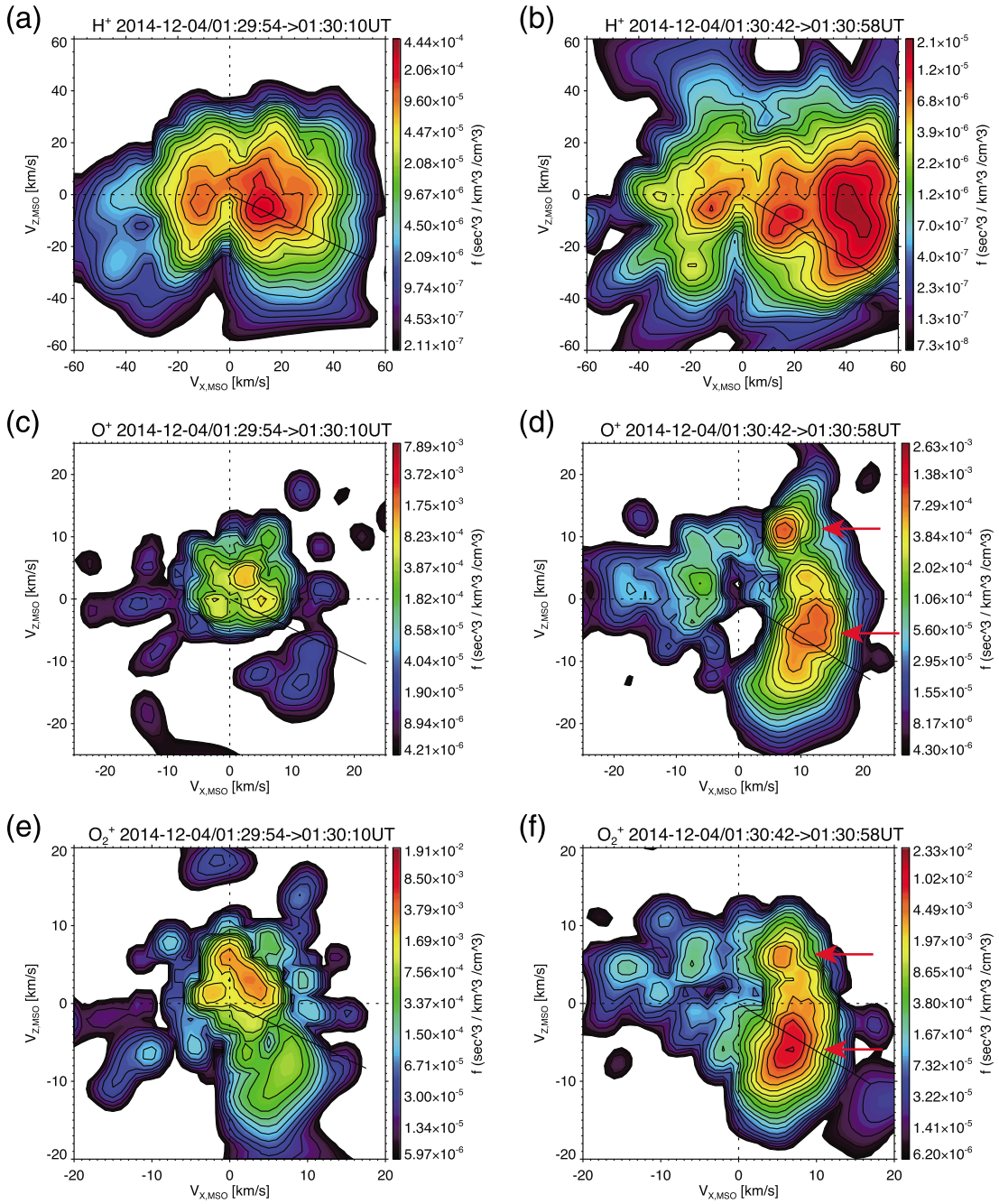

Figure 3. (a–f) Slices of ion velocity distribution functions on the $v_{x,MSO}$-$v_{z,MSO}$ plane at the times shown by vertical white lines in Figures 1d–1f. The black lines show the local magnetic field direction. The red arrows denote the counterstreaming beams separated along the current sheet normal ($\sim Z_{MSO}$) direction in the O^+ and O_2^+ ion distribution functions.

lines within the central tail current sheet, together with the negligible crustal field strength at this altitude, imply involvement of magnetic reconnection in creating a field line topology consistent with the ordering of the field directions that are observed.

In this closed field region within the central tail current sheet, STATIC measured enhanced Marsward bulk flows of the H^+, O^+, and O_2^+ ions (Figure 1h). The maximum X_{MSO} component of the bulk H^+ velocity ~26 km/s is comparable to the Alfvén velocity in the adjacent lobe region (Figure 1i), while the heavy ions exhibit smaller bulk acceleration of ~9 km/s for O^+ and ~6 km/s for O_2^+ ions. The Marsward Alfvénic flows within the current sheet suggest the presence of reconnection X lines tailward from the spacecraft. The mass

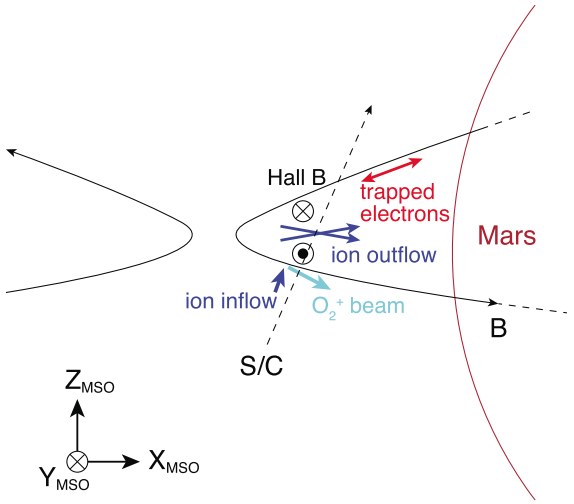

Figure 4. Schematic illustration of MAVEN observations of magnetic reconnection signatures in the near-Mars magnetotail.

dependence of ion outflow velocities will be discussed in the following section. We note that the O_2^+ energy spectra (Figure 1f) show the presence of two components just before the closed field region: low-energy cold ions with uncorrected energies of ~10 eV and a higher-energy beam component with an energy dispersion signature falling from ~100 eV at 01:28:46 UT to ~30 eV at 01:30:18 UT. The other two species do not exhibit as clear higher-energy populations as O_2^+ ions (Figures 1d and 1e).

Figure 2b shows the results of minimum variance analysis [*Sonnerup and Cahill*, 1967] at this current sheet crossing. The maximum (*i*), intermediate (*j*), and minimum (*k*) variance directions are almost along the X_{MSO}, Y_{MSO}, and Z_{MSO} axes, respectively. The hodograms exhibit a bipolar change in the intermediate-variance component as well as the presence of a large minimum variance component. The polarity of the bipolar signature has the correct signs for the tailward X line location [*Halekas et al.*, 2009]. The significant normal field across the current sheet also supports magnetic field topology of reconnection.

The details of the ion velocity distribution functions (VDFs) just before and inside the closed field region are shown in Figure 3. The spacecraft potential and velocity are corrected in these VDFs. The ion VDFs obtained just south of the closed field region (Figures 3a, 3c, and 3e) display the cold populations of H^+, O^+, and O_2^+ ions that are shifted northward (toward $+v_{z,MSO}$) by several km/s and are drifting perpendicularly to the local magnetic field direction. This drift direction is consistent with the cold ion inflow toward the current sheet from the southern tail lobe. The O_2^+ VDF additionally exhibits the aforementioned higher-energy beam component, which is traveling Marsward and southward (Figure 3e), suggesting that these higher-energy O_2^+ ions are escaping from the closed field region.

On the other hand, the ion VDFs inside the closed field region (Figures 3b, 3d, and 3f) show the intense Marsward flowing components on the $v_{x,MSO} > 0$ side. It is also seen that the H^+ VDF exhibits a broad distribution both in energy and angle (Figure 3b), while clear two peaks along the $v_{z,MSO}$ axis are resolved in the O^+ and O_2^+ VDFs as indicated by the red arrows in Figures 3d and 3f. These two peaks along $v_{z,MSO}$ with a $+v_{x,MSO}$ drift persist even when the local magnetic field changes its direction during this current sheet crossing (not shown), indicating the persistent presence of ion beams interpenetrating in the current sheet normal (Z_{MSO}) direction. Very similar interpenetrating ion beams separated nearly along the current sheet normal are found near the reconnection X line in the terrestrial plasma sheet [*Wygant et al.*, 2005] and in the ion diffusion regions reproduced by particle-in-cell simulations [*Liu et al.*, 2015]. Following these authors' terminology, hereafter we refer to these ion beams along Z_{MSO} as "counterstreaming" ions, though this term is often used to refer to field-aligned bidirectional beams, which are not necessarily the case here. We note that most of the O^+ and O_2^+ ions on the $v_{x,MSO} > 0$ side have negative $v_{y,MSO}$ components (not shown), which are consistent with Speiser-like acceleration by the cross-tail reconnection electric field. Another interesting population is the weaker tailward traveling ions on the $v_{x,MSO} < 0$ side (Figures 3b, 3d, and 3f), which could represent thermalized outflow populations or cold ions directly supplied from the nightside ionosphere along the connected field lines.

Assuming that the structure did not change during the MAVEN transit from 01:20:00 UT to 01:40:00 UT, the local current sheet width is ~520 km, corresponding to the distance along the current sheet normal traveled by the spacecraft. We obtain ion inertial lengths of ~174 km for H^+, ~363 km for O^+, and ~314 km for O_2^+ based on the average ion densities in the closed field region (Figure 1g). We also derive average local ion gyroradii of ~78 km for H^+, ~212 km for O^+, and ~214 km for O_2^+ from the local ion temperature and magnetic field magnitude. The local current sheet half thickness is comparable to the inertial lengths and gyroradii of O^+ and

O_2^+ ions, suggesting that the heavy ions are mostly demagnetized in the current sheet and that the spacecraft crossed the heavy ion diffusion regions.

Figure 4 summarizes the ion, electron, and magnetic field signatures observed by MAVEN at this current sheet crossing. The electron distributions indicate electron trapping in the closed field topology at the central tail current sheet. Just before the entry into the closed field region, the cold ion inflows drifting toward the current sheet are observed for all species. In addition, we observe the clear O_2^+ ion beam traveling Marsward and southward with energy dispersion. In the closed field region, we observe the intense Marsward flows of ions that have mass-dependent bulk velocities and are counterstreaming in the Z_{MSO} direction. The observed bipolar B_y signature changing from negative to positive signs has the consistent sense with the expected Hall magnetic field near reconnection diffusion regions. The combination of the electron, ion, and magnetic field measurements strongly suggests the presence of reconnection X lines located tailward from the spacecraft path.

3. Discussion

We first propose a possible interpretation of the observed mass-dependent bulk velocities and counterstreaming features of the reconnection outflow ions, based on previous simulations and observations in other environments. Multispecies, particle-in-cell simulations demonstrate that H^+ and O^+ ions can be accelerated by different mechanisms with different time scales in the reconnection outflow region [*Markidis et al.*, 2011; *Liu et al.*, 2015]. In their simulation results, lighter H^+ ions are remagnetized out of the H^+ diffusion region and coupled to the expelled magnetic field lines, leading to outflow acceleration along the current sheet; on the other hand, heavier O^+ ions are demagnetized within the larger O^+ diffusion region and delayed from the H^+ ions, accelerated mainly by Hall electric fields. In other words, heavy ions experience less effective magnetic drift and more dominant electric acceleration compared to protons. The inward acceleration by Hall electric fields at the separatrix regions results in interpenetrating/bouncing ions along the current sheet normal in the downstream ion diffusion region [*Drake et al.*, 2009; *Wygant et al.*, 2005]. Such inward electric fields were directly observed in the terrestrial plasma sheet together with H^+ and O^+ ions counterstreaming along the current sheet normal [*Wygant et al.*, 2005]. The counterstreaming ions, which are often observed as field-aligned bidirectional beams in the exhaust region, represent one of the most prominent signatures of kinetic ion behavior in reconnection exhausts and have been widely observed in the terrestrial plasma sheet [*Fujimoto et al.*, 1996; *Nagai et al.*, 2002], at the terrestrial magnetopause [*Phan et al.*, 2013], in the terrestrial magnetosheath [*Phan et al.*, 2007], and in the solar wind [*Gosling et al.*, 2005].

The MAVEN observations display the ion properties that are qualitatively consistent with the expected different behavior of protons and heavy ions caused by different effectiveness of inward electric field acceleration (counterstreaming beams in $v_{z,MSO}$) and magnetic drift (bulk flow in $v_{x,MSO}$) within the heavy ion diffusion regions. We observe clearly separated beams along $v_{z,MSO}$ with small drifts in $v_{x,MSO}$ for O^+ and O_2^+ ions (Figures 3d and 3f), while the H^+ slice shows the broader distribution and larger $v_{x,MSO}$ drift (Figure 3b). Strikingly similar characteristics, i.e., distinct counterstreaming O^+ beams with small v_x acceleration and broader, more v_x-accelerated H^+ distributions, are found in the simulated H^+ and O^+ VDFs in the downstream O^+ diffusion region [*Liu et al.*, 2015]. The mass-dependent behavior in the reconnection structure could be related to the presence of the dispersive O_2^+ beam in the absence of clear H^+ and O^+ beams just outside of the closed field region. Similar ion beams with energy dispersion in the separatrix regions are observed in the terrestrial magnetotail [*Machida et al.*, 1994; *Mukai et al.*, 1998] and in the solar wind [*Huttunen et al.*, 2008]. The abundance of planetary heavy ions in the near-Mars magnetotail provides us with a unique environment for investigation of multispecies aspects of magnetic reconnection processes.

Finally, we discuss the global context of this reconnection event. As mentioned in the previous section, the IMF switched its direction from northward to southward during the MAVEN tail crossing. The Marsward lobe field in the southern hemisphere before the current sheet crossing (Figure 2a) is consistent with the draping of the northward IMF. The Marsward field direction in the northern hemisphere after 01:41:26 UT (not shown) corresponds to the draping of the southward IMF. Therefore, it seems likely that the switched IMF reshaped the magnetotail configuration. Since we cannot tell exactly when the IMF orientation flipped without a continuous upstream IMF monitor, it remains uncertain whether this reconnection event took place in a stable, time-stationary current sheet or in a dynamic, time-variable magnetotail. Crustal magnetic fields might be implicated in the formation of the multiple closed fields (Figure 1b), but the spacecraft longitude in the

Mars body-fixed frame of ~124°W, which indicates the strong crustal field location far from the observed location, casts doubt on this interpretation.

We note that another type of reconnection signatures, a tail plasmoid with a magnetic flux rope, is expected to be observed in the farther downstream region relative to the reconnection site as observed in the Venusian tail [*Zhang et al.*, 2012]. Also, a quantitative assessment of the role of magnetic reconnection in atmospheric loss at Mars requires more information on the systematics of tail reconnection events such as their occurrence frequency as a function of upstream parameters and on the enhanced electromagnetic and particle energy flux to the ionosphere driven by reconnection. Statistical investigation of reconnection signatures as well as simulation studies for Martian tail reconnection will be necessary to fully address the local reconnection processes and their global consequences at Mars.

Acknowledgments
The authors wish to acknowledge great support from the team members of the MAVEN mission. This work was partially supported by the CNES for the part based on observations with the SWEA instrument embarked on MAVEN. MAVEN data are publicly available through the Planetary Data System.

The Editor thanks Brian Anderson and an anonymous reviewer for their assistance in evaluating this paper.

References

Beharrell, M. J., and J. A. Wild (2012), Stationary flux ropes at the southern terminator of Mars, *J. Geophys. Res.*, *117*, A12212, doi:10.1029/2012JA017738.

Brain, D. (2006), Mars global surveyor measurements of the Martian solar wind interaction, *Space Sci. Rev.*, *126*(1–4), 77–112, doi:10.1007/s11214-006-9122-x.

Brain, D. A., J. S. Halekas, L. M. Peticolas, R. P. Lin, J. G. Luhmann, D. L. Mitchell, G. T. Delory, S. W. Bougher, M. H. Acuña, and H. Rème (2006), On the origin of aurorae on Mars, *Geophys. Res. Lett.*, *33*, L01201, doi:10.1029/2005GL024782.

Brain, D. A., R. J. Lillis, D. L. Mitchell, J. S. Halekas, and R. P. Lin (2007), Electron pitch angle distributions as indicators of magnetic field topology near Mars, *J. Geophys. Res.*, *112*, A09201, doi:10.1029/2007JA012435.

Brain, D. A., A. H. Baker, J. Briggs, J. P. Eastwood, J. S. Halekas, and T.-D. Phan (2010), Episodic detachment of Martian crustal magnetic fields leading to bulk atmospheric plasma escape, *Geophys. Res. Lett.*, *37*, L14108, doi:10.1029/2010GL043916.

Briggs, J., D. Brain, M. Cartwright, J. Eastwood, and J. Halekas (2011), A statistical study of flux ropes in the Martian magnetosphere, *Planet. Space Sci.*, *59*(13), 1498–1505, doi:10.1016/j.pss.2011.06.010.

Connerney, J., J. Espley, P. L. Sheppard, and R. Oliverson (2014), The MAVEN magnetic field investigation, *Space Sci. Rev.*, doi:10.1007/s11214-015-0169-4.

Drake, J. F., M. Swisdak, T. D. Phan, P. A. Cassak, M. A. Shay, S. T. Lepri, R. P. Lin, E. Quataert, and T. H. Zurbuchen (2009), Ion heating resulting from pickup in magnetic reconnection exhausts, *J. Geophys. Res.*, *114*, A05111, doi:10.1029/2008JA013701.

Dubinin, E., M. Fraenz, A. Fedorov, R. Lundin, N. Edberg, F. Duru, and O. Vaisberg (2012a), Ion energization and escape on Mars and Venus, *Space Sci. Rev.*, *162*, 173–211, doi:10.1007/978-1-4614-3290-6_6.

Dubinin, E., M. Fraenz, J. Woch, T. L. Zhang, J. Wei, A. Fedorov, S. Barabash, and R. Lundin (2012b), Bursty escape fluxes in plasma sheets of Mars and Venus, *Geophys. Res. Lett.*, *39*, L01104, doi:10.1029/2011GL049883.

Dubinin, E., M. Fraenz, T. L. Zhang, J. Woch, Y. Wei, A. Fedorov, S. Barabash, and R. Lundin (2013), Plasma in the near Venus tail: Venus Express observations, *J. Geophys. Res. Space Physics*, *118*, 7624–7634, doi:10.1002/2013JA019164.

Eastwood, J. P., D. A. Brain, J. S. Halekas, J. F. Drake, T. D. Phan, M. Oieroset, D. L. Mitchell, R. P. Lin, and M. Acuña (2008), Evidence for collisionless magnetic reconnection at Mars, *Geophys. Res. Lett.*, *35*, L02106, doi:10.1029/2007GL032289.

Fujimoto, M., M. S. Nakamura, T. Nagai, T. Mukai, T. Yamamoto, and S. Kokubun (1996), New kinetic evidence for the near-Earth reconnection, *Geophys. Res. Lett.*, *23*(18), 2533–2536, doi:10.1029/96GL02429.

Gosling, J. T., R. M. Skoug, D. J. McComas, and C. W. Smith (2005), Direct evidence for magnetic reconnection in the solar wind near 1 AU, *J. Geophys. Res.*, *110*, A01107, doi:10.1029/2004JA010809.

Halekas, J. S., and D. A. Brain (2010), Global distribution, structure, and solar wind control of low altitude current sheets at Mars, *Icarus*, *206*(1), 64–73, doi:10.1016/j.icarus.2008.12.032.

Halekas, J. S., J. P. Eastwood, D. A. Brain, T. D. Phan, M. Oieroset, and R. P. Lin (2009), In situ observations of reconnection Hall magnetic fields at Mars: Evidence for ion diffusion region encounters, *J. Geophys. Res.*, *114*, A11204, doi:10.1029/2009JA014544.

Halekas, J. S., D. A. Brain, and J. P. Eastwood (2011), Large-amplitude compressive "sawtooth" magnetic field oscillations in the Martian magnetosphere, *J. Geophys. Res.*, *116*, A07222, doi:10.1029/2011JA016590.

Halekas, J. S., E. Taylor, G. Dalton, G. Johnson, D. Curtis, J. McFadden, D. Mitchell, R. Lin, and B. Jakosky (2013), The solar wind ion analyzer for MAVEN, *Space Sci. Rev.*, doi:10.1007/s11214-013-0029-z.

Hara, T., K. Seki, H. Hasegawa, D. A. Brain, K. Matsunaga, and M. H. Saito (2014a), The spatial structure of Martian magnetic flux ropes recovered by the Grad-Shafranov reconstruction technique, *J. Geophys. Res. Space Physics*, *119*, 1262–1271, doi:10.1002/2013JA019414.

Hara, T., K. Seki, H. Hasegawa, D. A. Brain, K. Matsunaga, M. H. Saito, and D. Shiota (2014b), Formation processes of flux ropes downstream from Martian crustal magnetic fields inferred from Grad-Shafranov reconstruction, *J. Geophys. Res. Space Physics*, *119*, 7947–7962, doi:10.1002/2014JA019943.

Huttunen, K. E. J., S. D. Bale, and C. Salem (2008), Wind observations of low energy particles within a solar wind reconnection region, *Ann. Geophys.*, *26*(9), 2701–2710, doi:10.5194/angeo-26-2701-2008.

Jakosky, B. M., et al. (2015), The Mars Atmosphere and Volatile Evolution (MAVEN) mission, *Space Sci. Rev.*, doi:10.1007/s11214-015-0139-x.

Krymskii, A. M., T. K. Breus, N. F. Ness, M. H. Acuña, J. E. P. Connerney, D. H. Crider, D. L. Mitchell, and S. J. Bauer (2002), Structure of the magnetic field fluxes connected with crustal magnetization and topside ionosphere at Mars, *J. Geophys. Res.*, *107*(A9), 1245, doi:10.1029/2001JA000239.

Liu, Y. H., C. G. Mouikis, L. M. Kistler, S. Wang, V. Roytershteyn, and H. Karimabadi (2015), The heavy ion diffusion region in magnetic reconnection in the Earth's magnetotail, *J. Geophys. Res. Space Physics*, *120*, 3535–3551, doi:10.1002/2015JA020982.

Lundin, R. (2011), Ion acceleration and outflow from Mars and Venus: An overview, *Space Sci. Rev.*, *162*(1–4), 309–334, doi:10.1007/s11214-011-9811-y.

Machida, S., T. Mukai, Y. Saito, T. Obara, T. Yamamoto, A. Nishida, M. Hirahara, T. Terasawa, and S. Kokubun (1994), GEOTAIL low energy particle and magnetic field observations of a plasmoid at $X_{GSM} = -142R_E$, *Geophys. Res. Lett.*, *21*, 2995–2998, doi:10.1029/94GL02241.

Markidis, S., G. Lapenta, L. Bettarini, M. Goldman, D. Newman, and L. Andersson (2011), Kinetic simulations of magnetic reconnection in presence of a background O^+ population, *J. Geophys. Res.*, *116*, A00K16, doi:10.1029/2011JA016429.

McFadden, J., et al. (2014), The MAVEN Suprathermal and thermal Ion Composition (STATIC) Instrument, *Space Sci. Rev.*

Mitchell, D. L., et al. (2014), The MAVEN Solar Wind Electron Analyzer (SWEA), *Space Sci. Rev.*

Morschhauser, A., V. Lesur, and M. Grott (2014), A spherical harmonic model of the lithospheric magnetic field of Mars, *J. Geophys. Res. Planets*, *119*, 1162–1188, doi:10.1002/2013JE004555.

Mukai, T., T. Yamamoto, and S. Machida (1998), Dynamics and kinetic properties of plasmoids and flux ropes: GEOTAIL observations, in *New Perspectives on the Earth's Magnetotail, Geophys. Monogr. Ser.*, vol. 105, edited by A. Nishida, D. N. Baker, and S. W. H. Cowley, pp. 117–137, AGU, Washington, D. C., doi:10.1029/GM105p0117.

Nagai, T., M. Nakamura, I. Shinohara, M. Fujimoto, Y. Saito, and T. Mukai (2002), Counterstreaming ions as evidence of magnetic reconnection in the recovery phase of substorms at the kinetic level, *Phys. Plasmas*, *9*(9), 3705–3711, doi:10.1063/1.1499117.

Nagy, A., et al. (2004), The plasma environment of Mars, *Space Sci. Rev.*, *111*(1–2), 33–114, doi:10.1023/B:SPAC.0000032718.47512.92.

Paschmann, G., M. Øieroset, and T. Phan (2013), In-situ observations of reconnection in space, *Space Sci. Rev.*, *178*(2–4), 385–417, doi:10.1007/s11214-012-9957-2.

Phan, T. D., G. Paschmann, C. Twitty, F. S. Mozer, J. T. Gosling, J. P. Eastwood, M. Øieroset, H. Rème, and E. A. Lucek (2007), Evidence for magnetic reconnection initiated in the magnetosheath, *Geophys. Res. Lett.*, *34*, L14104, doi:10.1029/2007GL030343.

Phan, T. D., G. Paschmann, J. T. Gosling, M. Oieroset, M. Fujimoto, J. F. Drake, and V. Angelopoulos (2013), The dependence of magnetic reconnection on plasma β and magnetic shear: Evidence from magnetopause observations, *Geophys. Res. Lett.*, *40*, 11–16, doi:10.1029/2012GL054528.

Sonnerup, B. U. Ö., and L. J. Cahill (1967), Magnetopause structure and attitude from Explorer 12 observations, *J. Geophys. Res.*, *72*(1), 171–183, doi:10.1029/JZ072i001p00171.

Wygant, J. R., et al. (2005), Cluster observations of an intense normal component of the electric field at a thin reconnecting current sheet in the tail and its role in the shock-like acceleration of the ion fluid into the separatrix region, *J. Geophys. Res.*, *110*, A09206, doi:10.1029/2004JA010708.

Zhang, T. L., et al. (2012), Magnetic reconnection in the near Venusian magnetotail, *Science*, *336*(6081), 567–570, doi:10.1126/science.1217013.